

# Effects of solar radiation pressure on asteroid surface hopping transfers for high area/mass ratio rovers

Chuan-Jun Dong, Hong-Wei Yang\*, Shuang Li and Xue-Wen Liu

College of Astronautics, Nanjing University of Aeronautics and Astronautics, Nanjing 210016, China;  
[hongwei.yang@nuaa.edu.cn](mailto:hongwei.yang@nuaa.edu.cn)

Received 2020 August 21; accepted 2021 January 23

**Abstract** The high area/mass ratio hopping rovers have potential applications in future asteroid surface exploration. This paper systematically investigates the effects of solar radiation pressure (SRP) on ballistic surface hopping transfers for the asteroid 101955 Bennu. Effects of SRP on the traveled distance and the trajectory design of hopping transfers are analyzed and summarized. The simulation results indicate that it is necessary to take SRP into account to ensure the success of hopping transfers and the proper use of SRP can help design the trajectories of hopping transfers with low initial impulses and short transfer times. It also reveals the potential possibility in using SRP to control the post-hopping transfers with specific control policies in the future surface exploration of asteroids.

**Key words:** asteroid — hopping — solar radiation pressure — dynamics — trajectory

## 1 INTRODUCTION

Asteroid exploration is becoming a popular topic in recent years. There are millions of asteroids with different shapes, sizes and compositions in the vast solar system (Margot et al. 2002; Yang et al. 2018). Exploration of asteroids and further landing on the surface can provide further insight into the origin problem, namely the origin of the solar system, Earth and life. Several famous exploring missions on small bodies have been successfully conducted. For instance, the spacecraft NEAR-Shoemaker was launched successfully by NASA (Veverka et al. 2001), which was the first asteroid-target exploring mission. Subsequently, the asteroid exploration interest continued worldwide. Rosetta and Hayabusa missions have tried to land on the surface of a comet and an asteroid, respectively. A lander named Philae carried by Rosetta was released to the surface of comet 67P/Churyumov-Gerasimenko (Biele et al. 2015). It was the first landing of a human-launched spacecraft on the surface of a comet. But the landing position of the Philae lander was not very ideal, and it finally settled down without sunlight. Hayabusa was the first asteroid sample return mission led by JAXA (Broschart & Scheeres 2005). Hayabusa released a 591g

small rover named MINERVA (Micro/Nano Experimental Robot Vehicle for Asteroid). However, the rover escaped from the surface of the asteroid 25143 Itokawa. Followed by the successful Hayabusa mission, Hayabusa-2 was launched successfully in 2014 and returned from target asteroid 162173 Ryugu after twice successful sampling (Tsuda et al. 2020; Yoshikawa et al. 2020). Another important asteroid sample return mission OSIRIS-REx led by NASA has explored the 101955 Bennu (Chesley et al. 2014; Lautetta et al. 2015). The probe investigated the chemical composition, mineral distribution and geological history of the asteroid. The information collected during the observation will help scientists understand how the sunlight affects the rotation of Bennu. Some important early detection results have already been obtained and samples will be taken to the Earth from the asteroid.

For the exploration missions of asteroids, landing or touching the surface of the target asteroid can help collect more accurate data. Much research has investigated the design of descent trajectories for asteroid landing (Pinson & Lu 2018; Yang et al. 2019; Yang & Li 2020). The surface environment of asteroids presents many unique challenges because the irregular shapes result in highly irregular gravity fields. The gravity of asteroids is much lower than planets, thus hopping rovers are regarded

---

\* Corresponding author

as an effective solution for asteroid surface exploration (Schwartz et al. 2017; Kalita et al. 2017). However, the surface exploration of the asteroid still remains a great challenge. Surface motions of asteroids have attracted the attention of researchers. Yu & Baoyin (2014) investigated the global motion strategy for particles on and above the surface of asteroids. Jiang et al. (2016) studied the surface motions by using a combination of an N-body gravity algorithm and a soft-sphere discrete element method. Zhang et al. (2019) studied the free motion of sample particles on and above the surface of Bennu. Wen et al. (2020) proposed the concept of hop reachable domain to evaluate the surface mobility of a hopping rover treated as a point mass. The design of hopping rovers is different from that of traditional planetary rovers. Canadian Space Agency studied the micro-hopper for Mars exploration which used hopping spring mechanism (Dupius et al. 2005) and MIT tried to use Polymer Actuator Membranes (PAM) to load a spring (Dubowsky et al. 2005; Kesner et al. 2007). Another technique is to use chemical and sublimate-based propulsion to perform hopping in low gravity environment (Thangavelautham et al. 2017).

Due to the weak gravity of asteroids, solar radiation pressure (SRP) is the primary perturbation for spacecraft dynamics around asteroids (Scheeres 2016). It is usually not negligible for analyzing the dynamics near asteroids. Many previous studies have investigated orbital dynamics around asteroids under the perturbation of SRP. For instance, terminator orbits (Dankowicz 1994; Byram & Scheeres 2009; Scheeres 2012; Feng & Hou 2019), hovering orbits (Sawai et al. 2002; Xin et al. 2016), delta-V assisted periodic orbits (Kikuchi et al. 2017), heliotropic orbits (Lantukh et al. 2015; Russell et al. 2016) and quasi-terminator orbits (Broschart et al. 2014). Solar sail spacecraft is the most common spacecraft using SRP for deep space exploration. The flight control of solar sail spacecraft does not rely on reaction propulsion (Tsuda et al. 2013). As for asteroid proximity missions, Zeng et al. (2016) investigated the body-fixed hovering over elongated asteroids. Recently, a future asteroid exploration concept Area-of-Effect Soft-bots (AoES) supported by NASA Innovative Advanced Concept (NIAC) program was proposed (McMahon 2018; McMahon et al. 2019). In their proposal, SRP can be used to propel the hopping rover which has a high area/mass ratio during the descent and hovering transfers. Hopping rovers like AoES have great potential applications in future asteroid exploration. Due to the high area/mass ratio of these rovers, the effects of SRP on the hopping transfers are expected to be non-negligible and needed to be analyzed. In McMahon (2018),

the effects of SRP on post-hopping landing points in a spherical gravitational field are preliminary investigated. In this paper, the effects of SRP on the asteroid-surface hopping transfer will be systematically analyzed. Bennu is chosen as the target asteroid which has an irregular gravitational field. In the analyses, the effects of SRP with different conditions of lift-off velocities and area/mass ratios will be investigated. Importantly, the effects of SRP on both the traveled distance and trajectory design of hopping transfers will be investigated.

First, the effects of SRP on the traveled distance of hopping transfers for asteroid's highly nonlinear gravity field are calculated and analyzed. Conditions of different lift-off velocities and area/mass ratios are also analyzed. Second, by changing the different parameters that affect SRP, the effects of SRP on the trajectory design of hopping transfers are also calculated and analyzed. In detail, the effects of the initial position of the Sun and the area/mass ratio on the hopping trajectories and the initial velocity are analyzed.

The organization of the rest of the paper is summarized as follows. Section 2 introduces the models and equations used in this paper briefly. In Section 3, the traveled distance maps of the hopping rover from different positions considering models with or without SRP are numerically simulated. The effective potential on the surface of Bennu is calculated. The effects on the trajectory design of hopping transfers under the perturbation of SRP are presented and analyzed in Section 4. Finally, the conclusion of this paper is provided in Section 5.

## 2 DYNAMICAL MODEL

### 2.1 Equation of Motion

The coordinate frames used are the inertial frame and the asteroid's body fixed frame illustrated in Figure 1.  $\hat{I} = \{\hat{I}_x \ \hat{I}_y \ \hat{I}_z\}$  is the inertial frame.  $\hat{b} = \{\hat{b}_x \ \hat{b}_y \ \hat{b}_z\}$  is the asteroid's body fixed frame, where  $\hat{b}_x$  is aligned with the minimum moment of inertia,  $\hat{b}_z$  is aligned with the maximum moment of inertia and  $\hat{b}_y$  completes the right-hand frame.  $\lambda$  is the initial position of the Sun with respect to the asteroid. The asteroid's rotational plane is assumed to coincide with its orbital plane. The asteroid rotates along the principal-axis  $\hat{b}_z$  at a constant angular velocity  $\omega$ . The direction cosine matrix  $[bI]$  is the elemental rotation matrix from the asteroid's inertial frame  $\hat{I}$  to the asteroid's body fixed frame  $\hat{b}$ :

$$[bI](t) = \begin{bmatrix} \cos \omega t & \sin \omega t & 0 \\ -\sin \omega t & \cos \omega t & 0 \\ 0 & 0 & 1 \end{bmatrix}. \quad (1)$$

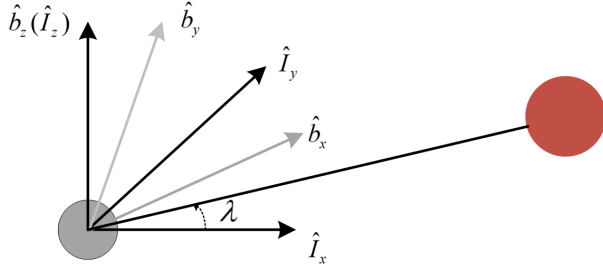


**Fig. 1** Inertial frame  $\hat{I}$  and the body fixed frame  $\hat{b}$ .

The equation of motion of the hopping rovers at position  $\mathbf{r}$  under the SRP perturbation in the asteroid's body fixed frame can be expressed as (Zeng et al. 2016):

$$\ddot{\mathbf{r}} + 2\boldsymbol{\omega} \times \dot{\mathbf{r}} + \boldsymbol{\omega} \times (\boldsymbol{\omega} \times \mathbf{r}) + \dot{\boldsymbol{\omega}} \times \mathbf{r} = \mathbf{g} + \mathbf{a}_{\text{SRP}}, \quad (2)$$

where  $\mathbf{g}$  is the asteroid's gravitational acceleration and  $\mathbf{a}_{\text{SRP}}$  is the disturbance acceleration caused by SRP. Assuming the angular velocity  $\boldsymbol{\omega}$  is constant, the motion Equation (2) can be simplified and written in its scalar components as:

$$\begin{bmatrix} \ddot{x} \\ \ddot{y} \\ \ddot{z} \end{bmatrix} = \begin{bmatrix} 2\omega\dot{y} + \omega^2x + g_x + a_{\text{SRP}x} \\ -2\omega\dot{x} + \omega^2y + g_y + a_{\text{SRP}y} \\ g_z + a_{\text{SRP}z} \end{bmatrix} \quad (3)$$

## 2.2 Gravity Field Model

The polyhedral model (Werner 1994; Werner & Scheeres 1996; Yu & Baoyin 2014), which is regarded as a high fidelity gravity model, is chosen to describe the irregular gravity near the surface of the target asteroid. The gravitational potential  $U$  and gravitational acceleration,  $\mathbf{g}=\nabla U$  then can be expressed as (Werner 1994):

$$U = -\frac{1}{2}G\rho \left( \sum_{e \in \text{Edge}} \mathbf{r}_e \cdot P_e(\mathbf{r}) - \sum_{f \in \text{Face}} \mathbf{r}_f \cdot Q_f(\mathbf{r}) \right), \quad (4)$$

$$\nabla U = G\rho \left( \sum_{e \in \text{Edge}} P_e(\mathbf{r}) - \sum_{f \in \text{Face}} Q_f(\mathbf{r}) \right), \quad (5)$$

where  $\rho$  is the bulk density of the asteroid,  $G$  is the gravitational constant,  $\nabla$  is the gradient operator,  $\mathbf{r}_e, \mathbf{r}_f$  are vectors from the field point to an arbitrary point on each edge and an arbitrary point on each face, and  $P_e$  and  $Q_f$  are defined as:

$$P_e(\mathbf{r}) = \begin{cases} 0 & \mathbf{r} \in e \\ \mathbf{E}_e \cdot \mathbf{r}_e \cdot L_e & \mathbf{r} \notin e \end{cases}, \quad (6)$$

$$Q_f(\mathbf{r}) = \begin{cases} 0 & \mathbf{r} \in f \\ \mathbf{F}_f \cdot \mathbf{r}_f \cdot \omega_f & \mathbf{r} \notin f \end{cases}. \quad (7)$$

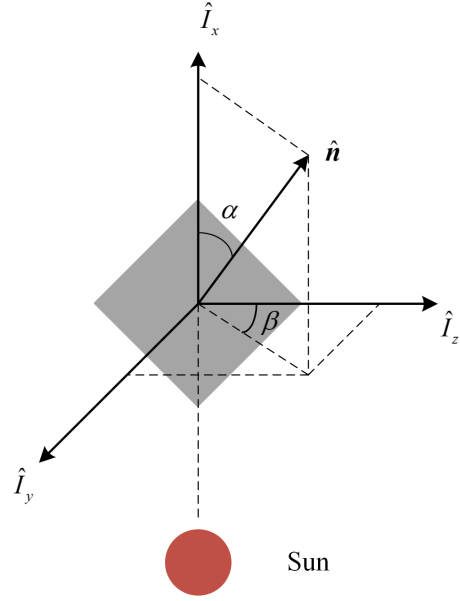


**Fig. 2** Attitude definition of the hopping rover.

$E_e$  and  $F_f$  are constant edge dyad and face dyad.  $L_e$  is an edge factor and  $\omega_f$  is the solid angle subtended by a face when viewed from the field point. The value of  $\omega_f$  can be used to verify that the position of the spacecraft is inside the asteroid or not.

$$V = U - \frac{1}{2}(\boldsymbol{\omega} \times \mathbf{r}) \cdot (\boldsymbol{\omega} \times \mathbf{r}). \quad (8)$$

The effective potential  $V$  in Equation (8) is an important physical property of asteroid (Zhang et al. 2019). It combines the centrifugal term and the gravitational potential of asteroids.

## 2.3 SRP Model

In the inertial frame  $\hat{I}$ , the hopping rover is assumed as a flat plate and a simple model to calculate the acceleration due to SRP is adopted. The attitude of the hopping rover is defined in the inertial frame  $\hat{I}$  by two angles: pitch angle  $\alpha$  and clock angle  $\beta$ , as shown in Figure 2.  $\alpha$  is defined as the angle between the direction of the sunlight and the normal direction of the hopping rover  $\hat{n}$ , and  $\beta$  is the angle between  $\hat{I}_z$  and the projection of  $\hat{n}$  on the plane perpendicular to  $\hat{I}_x$ . Regarding the hopping motion in the proximity of an asteroid, we assume the sun-rover vector is aligned to the sun-asteroid vector  $\hat{s}$ . SRP acceleration acting on the hopping rover is expressed as (McMahon 2018):

$$\mathbf{a} = a_0 \cos^2 \alpha \begin{bmatrix} \cos \alpha \\ -\sin \alpha \sin \beta \\ -\sin \alpha \cos \beta \end{bmatrix}, \quad (9)$$

$$a_0 = (2\eta P_0 \sigma) / d^2, \quad (10)$$

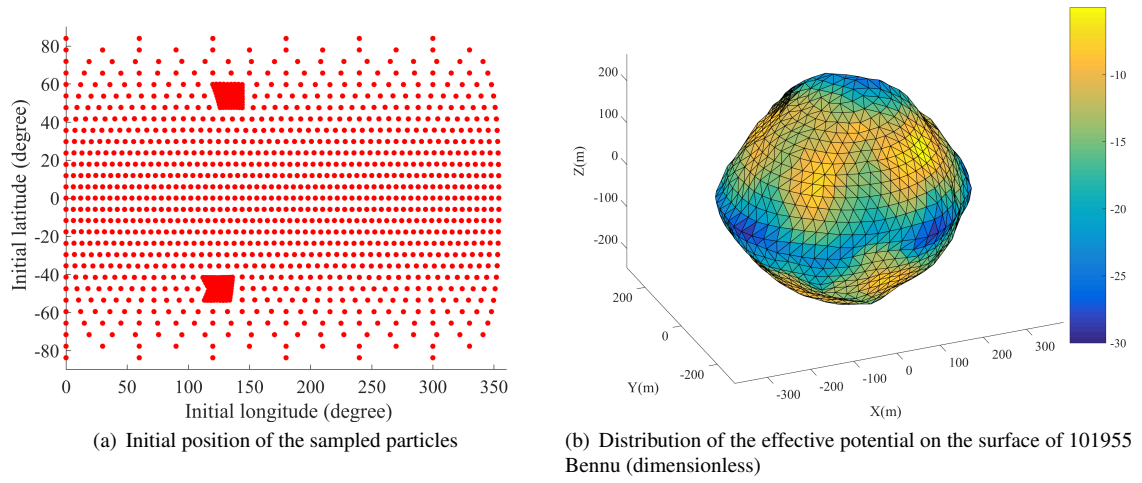


**Fig. 3** The initial position of the sampled particles and the distribution of the effective potential of the asteroid 101955 Benu.

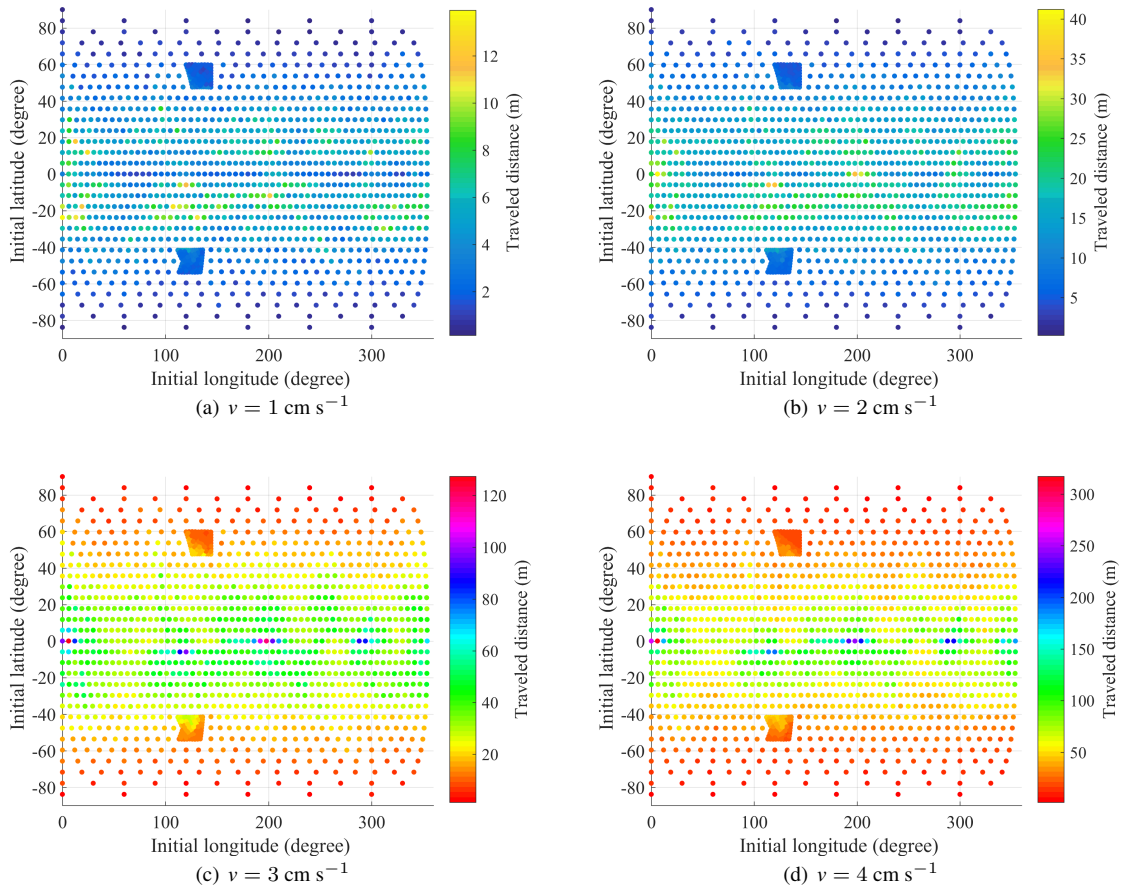


**Fig. 4** Traveled distance map for different velocity excluding SRP.

where  $d$  is the asteroid-sun distance,  $P_0$  is the solar constant,  $\sigma$  is area/mass ratio of hopping rover,  $0 \leq \alpha \leq \pi/2$ ,  $0 \leq \beta \leq 2\pi$  and  $\eta$  is the reflection coefficient of the hopping rover.

### 3 EFFECT OF SRP ON THE TRAVELED DISTANCE OF HOPPING TRANSFERS

This section investigates the effect of SRP on hopping transfers through comparison of the distribution of the

traveled distance with and without SRP. The target asteroid is chosen as 101955 Bennu, which is the target asteroid of the sample return mission OSIRIS-REx. Some parameters of the 101955 Bennu (Nolan et al. 2007; Nolan et al. 2013; Chesley et al. 2012) are shown in Table 1, where AU is the Astronomical Unit.

It has been demonstrated that SRP should not be sufficient to lift an object off the surface of a small body, but if a small impulse is given, hopping rovers can lift off from the surface of asteroids (McMahon 2018). Thus, a small impulse will be applied at the initial point for lifting off.

Throughout the following discussions, the reflection coefficient is assumed to be  $\eta = 0.8$  and the asteroid-sun distance  $d = 1.1264$  AU. The attitude of the hopping rover is assumed to a sun pointing attitude:  $\hat{\mathbf{n}} = \hat{\mathbf{s}}$  during the hopping motion process. For the convenience of analysis, in the body fixed frame of asteroid, the longitude  $\theta$  and the latitude  $\varphi$  are defined as:

$$\theta = \begin{cases} \arccos \frac{x}{\sqrt{x^2+y^2}} & y \geq 0 \\ 2\pi - \arccos \frac{x}{\sqrt{x^2+y^2}} & y < 0 \end{cases}, \quad (11)$$

and

$$\varphi = \arctan \frac{z}{\sqrt{x^2+y^2}}. \quad (12)$$

The distribution of sampled initial location is shown in Figure 3(a), where the initial positions are marked with dots and samples are generated as follows.

The position vectors  $\mathbf{r}$  are generated according to the 1348 vertices of polyhedral shape model. The initial velocity is set to be  $\dot{\mathbf{r}}_0 = v\mathbf{d}_0$ . The direction vector is defined as  $\mathbf{d}_0 = \frac{\mathbf{r}}{\|\mathbf{r}\|}$  and  $v$  is the magnitude of velocity.

### 3.1 Traveled Distance Excluding SRP

To illustrate the influence of hopping motion under the effect of asteroid's own irregular gravity. The hopping rover is set to lift off after different impulses have been applied. By lifting off from the position of the sampled particles in Figure 3(a), numerical results of traveled distance are summarized in Figure 4. The Euclidian distance between the lift-off location and the landing points is shown with a color chart. The traveled distance of hopping rover increases with the increase of the initial velocity. When the impulse has a magnitude of  $1 \text{ cm s}^{-1}$ , the maximum traveled distance is no more than 15 meters. But when the impulse is increased to a magnitude of  $4 \text{ cm s}^{-1}$ , the maximum traveled distance has already exceeded 300 meters. This is mainly because the escape velocity of asteroid Bennu is quite small, the minimum

**Table 1** 101955 Bennu Properties

Property	Value	Unit
Equivalent radius	246	m
Gravity parameter	5.2	$\text{m}^3 \text{s}^{-2}$
Rotation period	4.297812	h
Perihelion distance	0.8966	AU
Aphelion distance	1.3552	AU

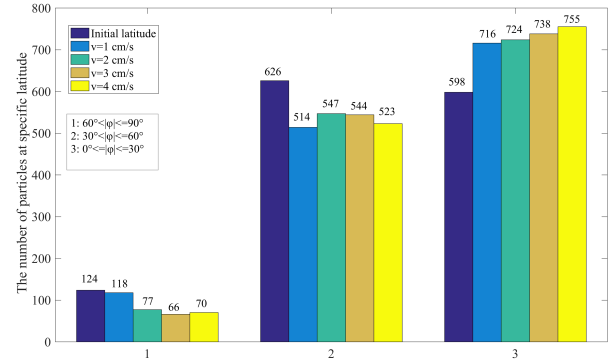


**Fig. 5** Distribution of particles for different initial velocity cases excluding SRP.

estimate of Bennu's escape velocity is  $v_{\text{esc}} = 13 \text{ cm s}^{-1}$  at the equator (Scheeres et al. 2016). So a small velocity change may cause a big difference in the movement state.

In addition, the distributions between the initial location and the final location are compared. The number of particles at specific latitude for different velocity is shown in Figure 5. It shows a tendency that the hopping rover tends to move from the high latitude area to the low latitude area after the hopping motion under the action of asteroid's own irregular gravity. This phenomenon could be meaningful for the exploration of asteroids' surface. For seeking the reason behind this interesting phenomenon, the distribution of the effective potential  $V$  on the surface of Bennu is calculated numerically. As the used polyhedral shape model has 2692 facets, to simplify the calculation, the effective potential of each facet's centroid is chosen to roughly represent the effective potential of that facet. The result is shown in Figure 3(b). The effective potential on the surface of asteroid Bennu shows a quite regular distribution. It presents a pattern where the effective potential changes with the latitude. The higher the latitude, the larger the effective potential. When in the low latitude, especially near the equator, it will have a much lower effective potential. That may explain the phenomenon that the hopping rover tends to move from the high latitude area to the low latitude area.

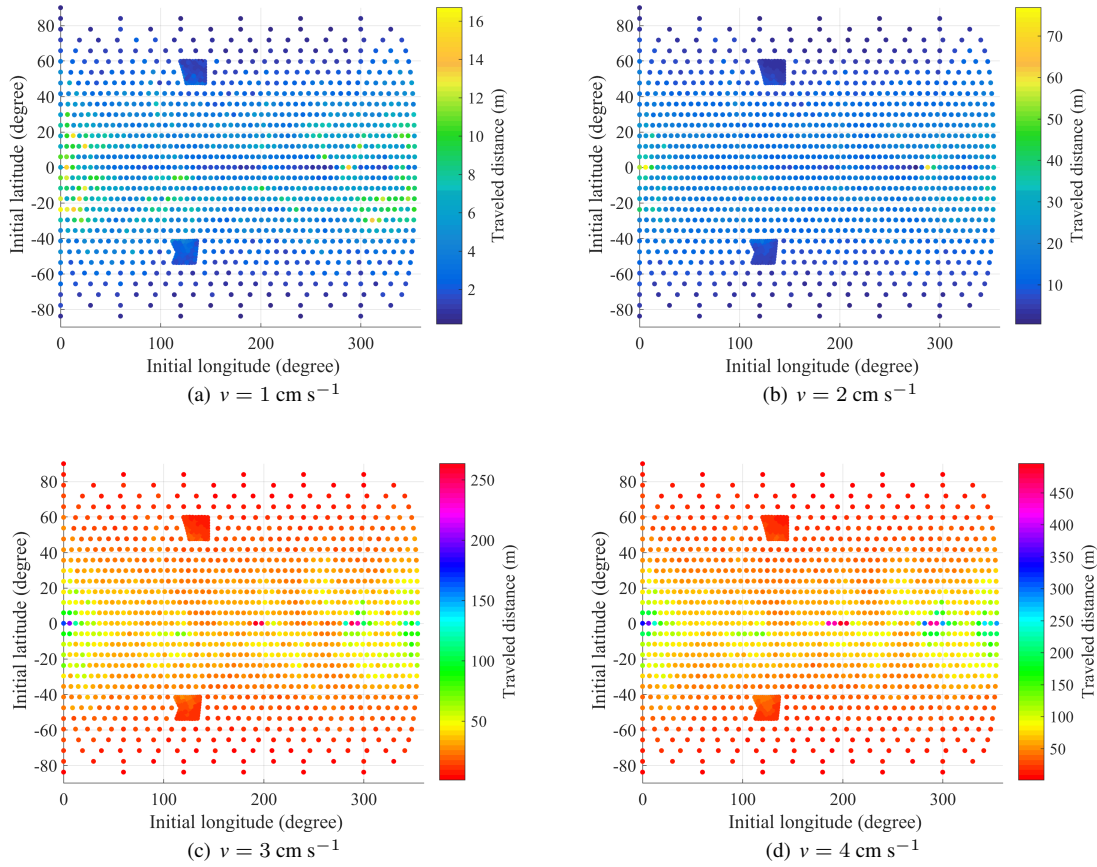


**Fig. 6** Traveled distance map for different velocity with SRP.

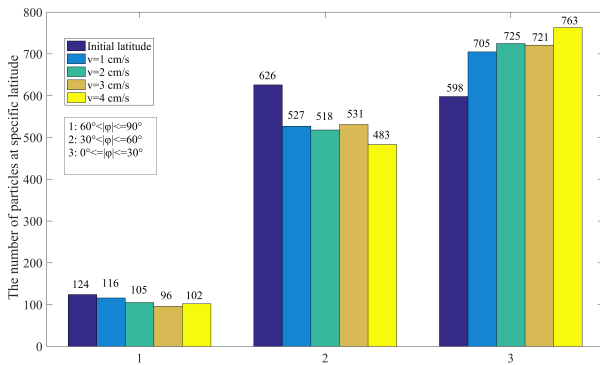


**Fig. 7** Distribution of particles for different initial velocity cases with SRP.

### 3.2 Traveled Distance with SRP

SRP is the primary perturbation for spacecraft dynamics near the surface of asteroids. Therefore, for the hopping motion on the surface of asteroids, SRP needs to be considered. The area/mass ratio of the hopping rover is assumed to be  $\sigma = 0.5 \text{ m}^2 \text{ kg}^{-1}$  (smaller than solar sails but larger than common spacecraft). The high area/mass ratio of the hopping rover may provide another important

capability to orbit and hopping trajectory control using SRP forces (McMahon et al. 2019). The numerical simulation results with SRP are presented in Figure 6. The same impulses of Section 3.1 are used in the numerical simulation for comparison. Similar to the result in Figure 5, Figure 7 also shows a tendency where the hopping rover tends to move from the high latitude area to the low latitude area after hopping motion under the action of asteroid's own irregular gravity and SRP. Comparing the traveled distance map of Figures 4 and 6, it shows that SRP does not change the distribution of traveled distance obviously when the imparted impulse is weak. But with the imparted impulse magnitude increasing, it presents different results. For instance, when the imparted impulse has a magnitude of  $v = 4 \text{ cm s}^{-1}$ , the final distribution of that traveled distance shows an obvious difference.

As can be seen from Figure 6, the maximum traveled distances are larger when considering the action of SRP by given different velocities. When the imparted impulse has a magnitude of  $1 \text{ cm s}^{-1}$ , the maximum traveled distance is no more than 15 meters in Figure 4(a). But it exceeds 15 meters in Figure 6(a) when the effects of SRP are involved.

For velocity  $v = 4 \text{ cm s}^{-1}$ , the maximum traveled distance changes from about 300 meters to exceed 450 meters when the action of SRP is turned on. This result may be quite reasonable because a larger impulse can make the hopping motion last a longer transfer time with the effect of SRP, so that SRP can act with more time. It shows that when the hopping rover lasts a long time hopping transfer SRP can influence the trajectories significantly. It will make the landing site deviate from the expected target position and may cause unexpected risk.

### 3.3 Parameter Study by Varying the Area/mass Ratio

Section 3.2 presented the numerical simulation results for the fixed area/mass ratio  $\sigma = 0.5 \text{ m}^2 \text{ kg}^{-1}$  when affected by SRP. However, it is an important factor of area/mass ratio in determining the magnitude of SRP acceleration as can be seen in Equation (10). In this section, the area/mass ratio of hopping rover will take six values of 0.1, 0.2, 0.3, 0.4, 0.5 and  $0.6 \text{ m}^2 \text{ kg}^{-1}$  to assess the influence of area/mass ratio, respectively. The initial velocity is set to be  $v = 4 \text{ cm s}^{-1}$ , because a larger impulse can make SRP's effect more significant.

Figure 8 shows the distribution of the traveled distance for different area/mass ratios. The traveled distance pattern differs with the change of area/mass ratio. As the area/mass ratio increases, the maximum traveled distance increases first and then decreases. The trajectories corresponding to the maximum traveled distance with different area/mass ratios are shown in Figure 9. The transfer time is also presented in Figure 9. The transfer time increases as the area/mass ratio increases. Longer transfer time leads to a larger traveled distance at first. But when the transfer time reaches a certain level, the longer trajectory has crossed the surface of the asteroid and the final landing point is closer to the initial point, which leads to the decrease of the traveled distance. This phenomenon shows that the change of area/mass ratio can be used to alter the action of SRP and further change the hopping motion trajectories of hopping rover. It shows a potential possibility to use SRP to guide around the small bodies like Benu in the future exploration.

## 4 EFFECT OF SRP ON THE TRAJECTORY DESIGN OF HOPPING TRANSFERS

Simulations of proposed hopping transfers on the surface of Benu are made in this section. The previous results show that, when the hopping rover is given an impulse in different directions and lifts off from different locations, it tends to approach the equatorial region under the asteroid

Benu's irregular gravity because the effective potential is relatively lower there. Zhang et al. (2019) pointed out that free motion of particles with zero initial velocities on the surface of Benu tends to stop finally in the low latitude areas, regardless of their initial positions. A similar conclusion can also be found from the related research work from Van Wal & Scheeres (2017). Due to this phenomenon, the low latitude areas of Benu may be suitable for landing and starting the transfer. So a hopping transfer mission near the equatorial region is simulated.

The maneuver is treated as an impulsive process and performed at the initial position. The initial position P1 is located on the vertex of the polyhedron shape model and the terminal position P2 is located on the facet. The problem of calculating the launch velocity  $\mathbf{v}$  to arrive a target location  $\mathbf{r}_f$  at transfer time  $t$  is the well-known *Lambert orbital boundary-value problem* (TPBVP) (Kalita & Thangavelautham 2019). The method used in this paper is the shooting method. For the highly nonlinear gravity field of Benu, first the initial guess velocity  $\mathbf{v}_0$  was obtained by solving the TPBVP with the spherical gravity field. For the  $i^{\text{th}}$  iteration in the shooting process, the initial velocity vector is changed as:

$$\mathbf{v}_{0(i+1)} = \mathbf{v}_{0(i)} + \Delta\mathbf{v}, \quad (13)$$

$$\Delta\mathbf{v} = [\Phi]^{-1} \Delta\mathbf{r}, \quad (14)$$

$$\Delta\mathbf{r} = \mathbf{r}_f - \mathbf{r}_n, \quad (15)$$

$$\Phi = \begin{bmatrix} \frac{\partial \mathbf{r}}{\partial \mathbf{v}_0} \end{bmatrix} = \begin{bmatrix} \frac{\partial x}{\partial \dot{x}_0} & \frac{\partial x}{\partial \dot{y}_0} & \frac{\partial x}{\partial \dot{z}_0} \\ \frac{\partial y}{\partial \dot{x}_0} & \frac{\partial y}{\partial \dot{y}_0} & \frac{\partial y}{\partial \dot{z}_0} \\ \frac{\partial z}{\partial \dot{x}_0} & \frac{\partial z}{\partial \dot{y}_0} & \frac{\partial z}{\partial \dot{z}_0} \end{bmatrix}, \quad (16)$$

where  $\Phi$  is the state transition matrix,  $\mathbf{r}_f$  is the desired final position and  $\mathbf{r}_n$  is the final position vector calculated by the numerical integration of the equations of motion. If the difference is less than a specified tolerance, this process then stops and the solution of initial velocity is found.

When SRP is excluded, Figure 10 plots the trajectories with the minimum and maximum initial velocity from P1 =  $[-244.935, 108.745, -27.8] \text{ m}$  to P2 =  $[-221.649, 138.652, -5.133] \text{ m}$ .

To investigate the influence of SRP in the process of hopping transfers, two constraints are used in the simulations. One constraint is the area/mass ratio of the hopping rover, which is set to: 0.1, 0.3 and  $0.5 \text{ m}^2 \text{ kg}^{-1}$ , respectively. The other constraint is the initial position of the Sun at the beginning of the hopping transfer as shown in Figure 1. Four angles  $\lambda$  are taken into account, which are 0 degree, 90 degrees, 180 degrees and 270 degrees, respectively.

When SRP is considered during the hopping motion, the minimum initial launch velocity is chosen to verify its

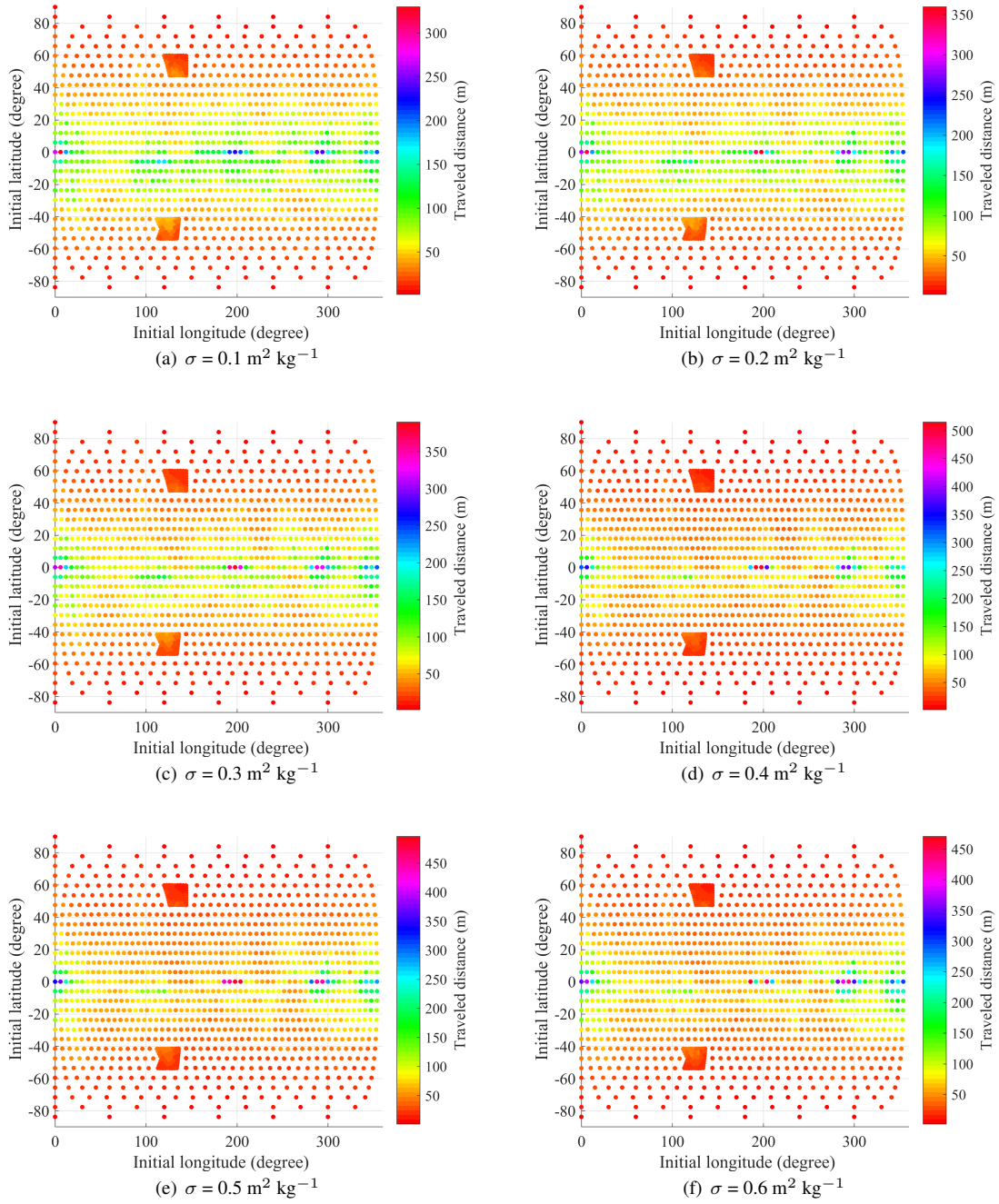


**Fig. 8** Traveled distance map for different area/mass ratio cases.

**Table 2** Distance Deviation From P2 and the Corresponding Transfer Time

	$\sigma = 0.1 \text{ m}^2 \text{ kg}^{-1}$		$\sigma = 0.3 \text{ m}^2 \text{ kg}^{-1}$		$\sigma = 0.5 \text{ m}^2 \text{ kg}^{-1}$	
	d(m)	time(h)	d(m)	time(h)	d(m)	time(h)
Excluding SRP	0.000	0.539	0.000	0.539	0.000	0.539
Sun at 0 deg	1.292	0.553	2.841	0.626	5.286	0.674
Sun at 90 deg	0.911	0.542	2.347	0.614	4.741	0.656
Sun at 180 deg	0.878	0.534	1.962	0.602	3.946	0.643
Sun at 270 deg	1.572	0.572	2.572	0.621	5.167	0.668

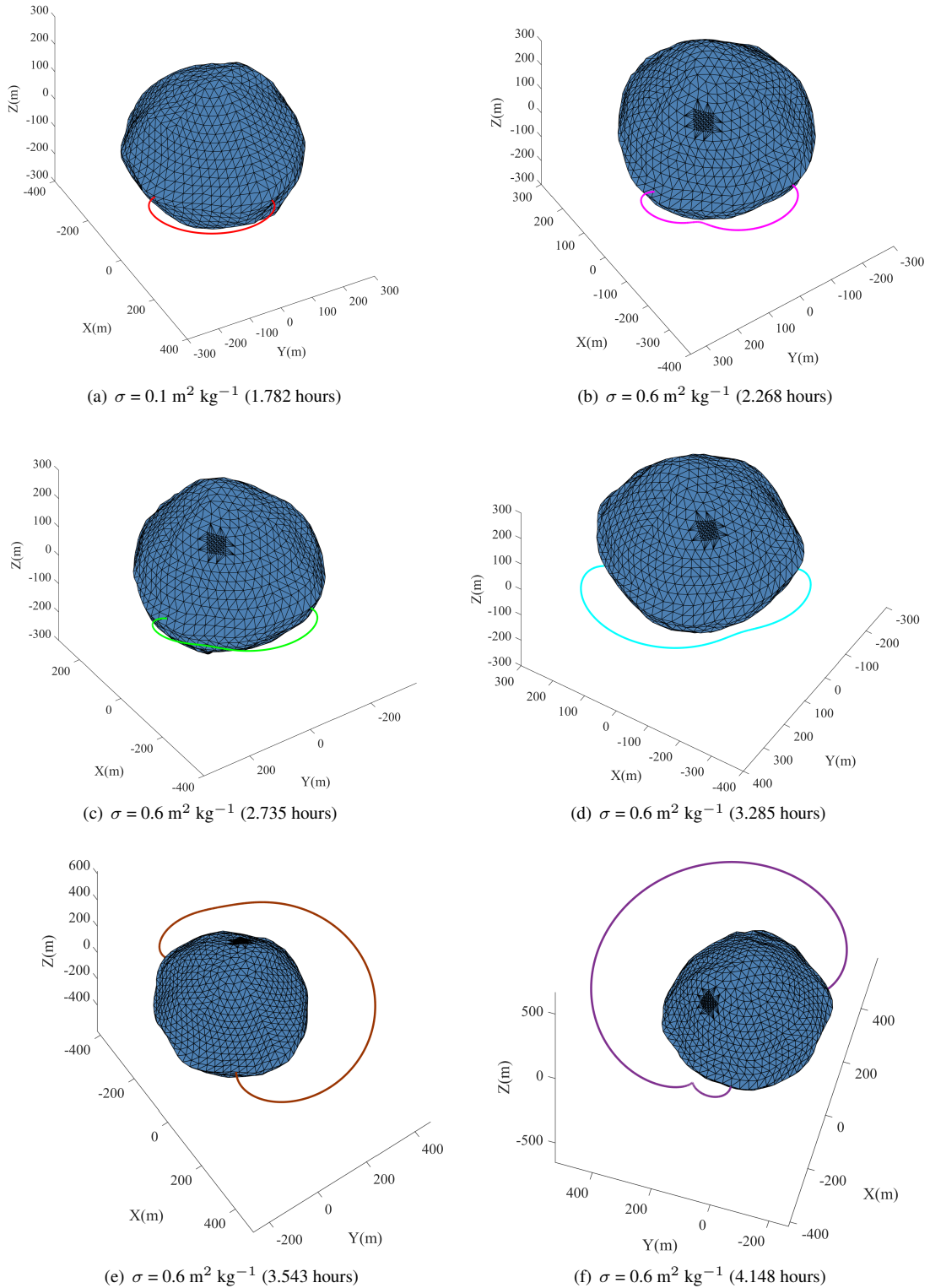


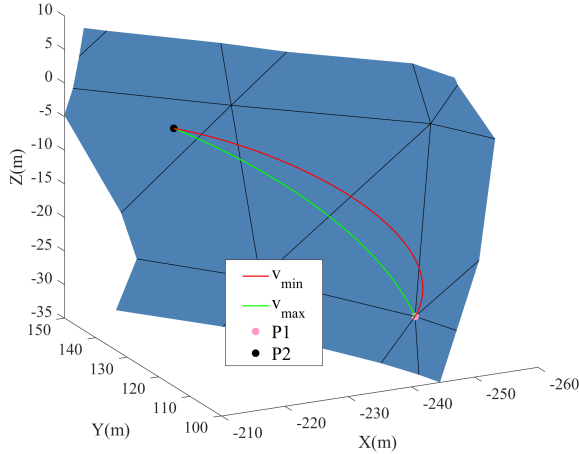
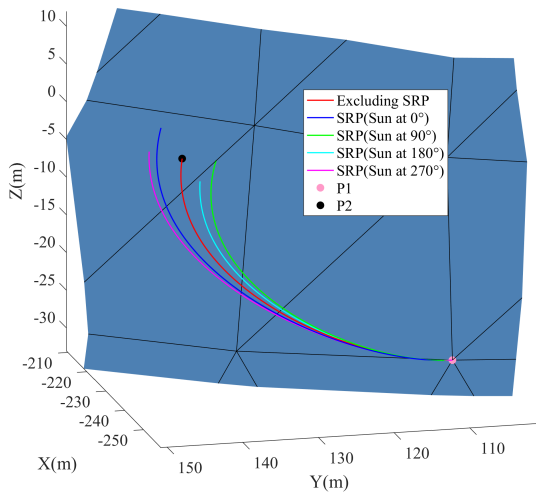
**Fig. 9** Trajectories of the maximum traveled distance for different area/mass ratio cases.

effects. Figure 11 indicates how trajectories are influenced when the action of SRP is turned on. The deviation of distance between P2 and the final landing point and the corresponding transfer time are calculated in Table 2

to show the effects of the SRP specifically. For  $\sigma = 0.1 \text{ m}^2 \text{ kg}^{-1}$ , the distance deviation varies from 0.878 to 1.572 m. The distance deviation increases as the  $\sigma$

**Table 3** The Minimum Initial Velocity and the Corresponding Transfer Time

	$\sigma = 0.1 \text{ m}^2 \text{ kg}^{-1}$		$\sigma = 0.3 \text{ m}^2 \text{ kg}^{-1}$		$\sigma = 0.5 \text{ m}^2 \text{ kg}^{-1}$	
	$v(\text{cm s}^{-1})$	time(h)	$v(\text{cm s}^{-1})$	time(h)	$v(\text{cm s}^{-1})$	time(h)
Excluding SRP	3.56	0.539	3.56	0.539	0.000	0.539
Sun at 0 deg	3.52	0.544	3.48	0.547	3.38	0.554
Sun at 90 deg	3.62	0.534	3.68	0.529	3.78	0.523
Sun at 180 deg	3.61	0.536	3.66	0.529	3.72	0.526
Sun at 270 deg	3.51	0.544	3.45	0.549	3.35	0.559

**Fig. 10** Hopping trajectories from P1 to P2 with  $v_{\min}$  and  $v_{\max}$ .**Fig. 11** Hopping trajectories from P1 to P2 with SRP for  $\sigma = 0.5 \text{ m}^2 \text{ kg}^{-1}$ .

increases. When  $\sigma = 0.5 \text{ m}^2 \text{ kg}^{-1}$ , the maximum distance deviation reaches 5.286 m.

Besides, the distance deviation also changes with the initial position of the Sun. The differences between different area/mass ratios increase with the transfer time. The distance deviation changes as transfer time changes. A longer transfer time makes a larger distance deviation

in Table 2. The transfer time will be influenced by the area/mass ratio and the initial position of the Sun. The factors will affect SRP and further affect the hopping motion to a certain extent. The hopping rover may not reach the final P2 due to the influence of SRP.

From the simulations results above, SRP should be taken into account. Otherwise the hopping rover may not reach the final position accurately. Next simulations present the real value of the required minimum initial velocity when SRP is included to reach the ideal position accurately.

The minimum initial velocity magnitude  $v_{\min}$  required is compared in Figure 12. The results for the case without SRP are used as a basic reference data. It is presented with a horizontal line, which is  $3.56 \text{ cm s}^{-1}$  in the hopping transfer from P1 to P2. The  $v_{\min}$  changes more drastically with a higher area/mass ratio. For  $\sigma = 0.5 \text{ m}^2 \text{ kg}^{-1}$ ,  $v_{\min}$  varies from  $3.35$  to  $3.78 \text{ cm s}^{-1}$  and the difference is  $0.43 \text{ cm s}^{-1}$ .

The basic reference values of the minimum initial velocity and the corresponding transfer time without SRP are compared in Table 3. The initial impulse magnitude and the transfer time could be changed with different area/mass ratios and initial position of the Sun. According to the results, SRP can help design the hopping transfer trajectories with lower initial velocities and shorter transfer times. For different area/mass ratio, the varying tendency of the minimum initial velocity with respect to the change of the initial position of the Sun is the same. Table 3 presents the transfer time corresponding to the minimum initial velocity. It shows that initial velocity increases as the transfer time decreases. The transfer time is influenced by the area/mass ratio and the initial position of the Sun at the same time. It is possible to design a more reasonable and flexible transfer trajectory for different situations. These results demonstrate that SRP can be used in a positive way when designing hopping transfer trajectories on the asteroid's surface, and show the potential applications of SRP in guidance around the asteroids in the future.

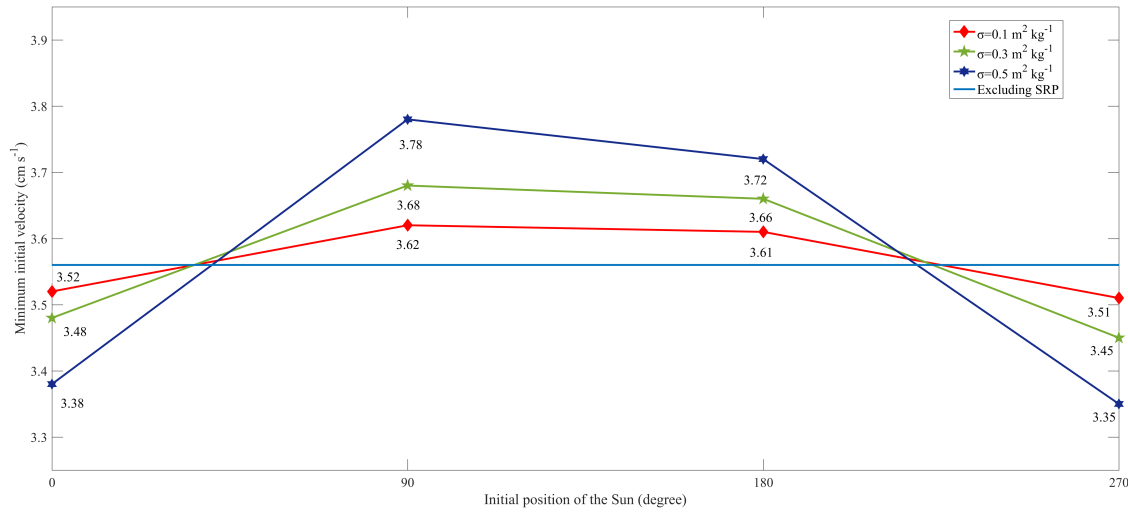


**Fig. 12** The minimum initial velocity required with SRP.

## 5 CONCLUSIONS

In this paper, the effects of SRP to the hopping motion on the surface of asteroid are studied. Regardless of different latitudes of the initial position of the hopping rover, the number of particles at specific latitude for the cases with or without SRP shows that the hopping rover tends to hop towards low latitude area. Compared with the case without SRP, the distribution of the traveled distance of the case with SRP shows that the maximum traveled distance changes from about 300 meters to exceed 450 meters when the initial velocity  $v = 4 \text{ cm s}^{-1}$  and the area/mass ratio  $\sigma = 0.5 \text{ m}^2 \text{ kg}^{-1}$ . Significant differences for the traveled distance are also noticed between the cases with and without SRP when the conditions of initial velocity and area/mass ratio are changed. These simulation results indicate the importance to consider SRP's effects for hopping transfers on the surface of asteroids. In addition, a proposed hopping transfer process is studied to assess the effects of SRP on trajectory design. The numerical simulations show that it is necessary to attach importance to the influence of SRP. Otherwise the hopping rover may not reach the desired position and may cause unexpected risk. The initial velocity required and the transfer time change with both the area/mass ratio and the initial position of the Sun. SRP can be used positively to lower the initial velocity and the transfer time. These results reveal the potential possibility in using SRP to explore on the surface of small asteroids like Bennu and it can provide control for the post-hopping transfers in the future exploration of asteroids.

**Acknowledgements** The work described in this paper was supported by the Fundamental Research Funds for the Central Universities (No. NS2019053).

## References

- Biele, J., Ulamec, S., Maibaum, M., et al. 2015, *Science*, 349, 6247
- Broschart, S. B., Lantoine, G., & Grebow, D. J. 2014 *Celestial Mechanics and Dynamical Astronomy*, 120, 195
- Broschart, S. B., & Scheeres, D. J. 2005, *Journal of Guidance Control and Dynamics*, 28, 343
- Byram, S. M., & Scheeres, D. J. 2009, *Journal of Guidance, Control, and Dynamics*, 32, 1550
- Chesley, S. R., Farnocchia, D., Nolan, M. C., et al. 2014, *Icarus*, 235, 5
- Chesley, S. R., Nolan, M. C., Farnocchia, D., et al. 2012, *AAS/Division of Dynamical Astronomy Meeting*, 43, 7.08
- Dankowicz, H. 1994, *Celestial Mechanics and Dynamical Astronomy*, 58, 353
- Dubowsky, S., Iagnemma, K., Liberatore, S., et al. 2005, *AIP Conference Proceedings*, American Institute of Physics, 746, 1449
- Dupius, E., Montminy, S., & Allard, P. 2005, *The 8th International Symposium on Artificial Intelligence, Robotics and Automation in Space*, ESA SP-603, 38
- Feng, J., & Hou, X. Y. 2019, *Communications in Nonlinear Science and Numerical Simulation*, 76, 71
- Jiang, Y., Zhang, Y., & Baoyin, H. 2016, *Planetary and Space Science*, 127, 33
- Kalita, H., Nallapu, R. T., Warren, A., et al. 2017, preprint (arXiv:1701.07550)
- Kalita, H., & Thangavelautham, J. 2019, preprint (arXiv:1902.02065)

- Kesner, S. B., Plante, J. S., Boston, P. J., et al. 2007, Proceedings 2007 IEEE International Conference on Robotics and Automation. IEEE, 4893
- Kikuchi, S., Tsuda, Y., & Kawaguchi, J. 2017, Journal of Guidance, Control, and Dynamics, 40, 150
- Lantukh, D., Russell, R. P., & Broschart, S. 2015, Celestial Mechanics and Dynamical Astronomy, 121, 171
- Lauretta, D. S., Bartels, A. E., Barucci, M. A., et al., 2015, Meteoritics and Planetary Science, 50, 834
- Margot, J., Nolan, M. C., Benner, L. A., et al., 2002, Science, 296, 1445
- McMahon, J., Mitchell, S. K., Oguri, K., et al. 2019, IEEE Aerospace Conference, 1
- McMahon, J. 2018, Dismantling Rubble Pile Asteroids with AoES (area-of-effect soft-bots)<https://ntrs.nasa.gov/citations/20180006790>
- Nolan, M. C., Magri, C., Howell, E. S., et al. 2013, Icarus, 226, 629
- Nolan, M. C., Magri, C., Ostro, S. J., et al. 2007, Bulletin of the American Astronomical Society, 39, 433
- Pinson, R., & Lu, P. 2018, Journal of Guidance, Control, and Dynamics, 41, 6
- Russell, R. P., Lantukh, D., & Broschart, S. B. 2016, Journal of Guidance, Control, and Dynamics, 39, 9
- Sawai, S., Scheeres, D. J., & Broschart, S. B. 2002, Journal of Guidance, Control, and Dynamics, 25, 786
- Scheeres, D. J., Hesar, S. G., Tardivel, S., et al. 2016, Icarus, 276, 116
- Scheeres, D. J. 2012, Journal of Guidance, Control, and Dynamics, 35, 987
- Scheeres, D. J. 2016, Orbital motion in Strongly Perturbed Environments: Applications to Asteroid, Comet and Planetary Satellite Orbiters (Springer)
- Schwartz, S. R., Asphaug, E., Raura, L., et al. 2017, in Lunar and Planetary Science Conference, 2781
- Thangavelautham, J., Robinson, M. S., Tait, A., et al. 2017, preprint (arXiv:1701.07799)
- Tsuda, Y., Mori, O., Funase, R., et al. 2013, Acta Astronautica, 82, 183
- Tsuda, Y., Takeuchi, H., Ogawa, N., et al. 2020, Astrodynamics, 4, 137, <https://doi.org/10.1007/s42064-020-0074-9>
- Van Wal, S., & Scheeres, D. J. 2017, Journal of Guidance, Control, and Dynamics, 40, 1990
- Veverka, J., Farquhar, B., Robinson, M. S., et al. 2001, Nature, 413, 390
- Wen, T., Zeng, X., Circi, C., & Gao, Y. 2020, Journal of Guidance, Control, and Dynamics, 43, 1269
- Werner, R. A., & Scheeres, D. J. 1996, Celestial Mechanics and Dynamical Astronomy, 65, 313
- Werner, R. A. 1994, Celestial Mechanics and Dynamical Astronomy, 59, 253
- Xin, X., Scheeres, D. J., & Hou, X. 2016, Celestial Mechanics and Dynamical Astronomy, 126, 405
- Yang, H., Li, S., & Bai, X. 2019, Journal of Guidance, Control, and Dynamics, 42, 585
- Yang, H., Li, S., Xu, C., et al. 2018, RAA (Research in Astronomy and Astrophysics), 18, 7
- Yang, H., & Li, S. 2020, IEEE Transactions on Aerospace and Electronic Systems, 56, 4338
- Yoshikawa, K., Sawada, H., Kikuchi, S., et al. 2020, Astrodynamics, 4, 119, <https://doi.org/10.1007/s42064-020-0073-x>
- Yu, Y., & Baoyin, H. X., 2014, Acta Mechanica Sinica, 30, 301
- Zeng, X., Gong, S., Li, J., & Alfriend, K. T. 2016, Journal of Guidance, Control, and Dynamics, 39, 1223
- Zhang, Y., Zeng, X., Circi, C., et al. 2019, Acta Astronautica, 163, 3